

Kerstin Wörhoff\*, René G. Heideman, Arne Leinse and Marcel Hoekman

# TriPleX: a versatile dielectric photonic platform

**Abstract:** Photonic applications based on planar waveguide technology impose stringent requirements on properties such as optical propagation losses, light coupling to optical fibers, integration density, as well as on reliability and reproducibility. The latter is correlated to a high level of control of the refractive index and waveguide geometry. In this paper, we review a versatile dielectric waveguide platform, called TriPleX, which is based on alternating silicon nitride and silicon dioxide films. Fabrication with CMOS-compatible equipment based on low-pressure chemical vapor deposition enables the realization of stable material compositions being a prerequisite to the control of waveguide properties and modal shape. The transparency window of both materials allows for the realization of low-loss waveguides over a wide wavelength range (400 nm–2.35  $\mu\text{m}$ ). Propagation losses as low as  $5 \times 10^{-4}$  dB/cm are reported. Three basic geometries (box shell, double stripe, and filled box) can be distinguished. A specific tapering technology is developed for on-chip, low-loss (<0.1 dB) spotsize convertors, allowing for combining efficient fiber to chip coupling with high-contrast waveguides required for increased functional complexity as well as for hybrid integration with other photonic platforms such as InP and SOI. The functionality of the TriPleX platform is captured by verified basic building blocks. The corresponding library and associated design kit is available for multi-project wafer (MPW) runs. Several applications of this platform technology in communications, biomedicine, sensing, as well as a few special fields of photonics are treated in more detail.

**Keywords:** dielectric; low-loss waveguide; microwave photonics; spotsize convertor.

DOI 10.1515/aot-2015-0016

Received January 30, 2015; accepted March 6, 2015

\*Corresponding author: Kerstin Wörhoff, Lionix BV, P.O. Box 456, 7500 AL, Enschede, The Netherlands, e-mail: k.worhoff@lionixbv.nl  
René G. Heideman, Arne Leinse and Marcel Hoekman: Lionix BV, P.O. Box 456, 7500 AL, Enschede, The Netherlands

[www.degruyter.com/aot](http://www.degruyter.com/aot)

 ©2015, Kerstin Wörhoff et al., published by De Gruyter.

This work is licensed under the Creative Commons Attribution-NonCommercial-NoDerivatives 3.0 License.

## 1 Introduction

Over the past decades integrated optics solutions for communications and sensing have rapidly developed and became increasingly important for the telecommunication market, space applications, in environmental control, as well as healthcare and life science [1–3].

In general, the applied photonics technology has to fulfill requirements such as low optical propagation losses, efficient light coupling to optical fibers, high integration density, low cost, manufacturability, and combining excellent performance of passive photonic circuitry with access to active functionality for light generation, detection, and modulation. However, the quantification of these demands in terms of transmission loss limits, applicable wavelength ranges, cost price, and manufacturing scale are rather diverse for the different application fields.

For the telecommunication market, the ever-increasing demand for capacity can be fulfilled by the steadily developing optical fiber networks. Consequently, similar performance requirements rise for switching and routing functionalities leading to the replacements of electronics by optical components for signal processing [4–6]. Examples of integrated photonic solutions are demonstrated in microwave photonics (MWP) [7, 8], network components for fiber-to-the-home (FTTH) [9, 10], and datacom applications [11–13]. For compatibility with the existing fiber backbone, Telecom and FTTH applications require wavelength ranges at 1.3–1.55  $\mu\text{m}$ , while for datacom applications, the availability of low-cost, high-speed modulating VCSELs is of importance. Operating wavelengths for the latter application field are either 850 nm (multimode fiber links in rack to rack connections) or 1.3  $\mu\text{m}$  (single-mode fiber connections in large-scale datacenters). Besides performance and reliability, cost per bit of transmitted data and potential for large-scale manufacturability are key requirements of this market segment. To date, the breakthrough of photonic components is being hampered, however, by high cost due to large optical footprint (i.e., chip real estate) and costly packaging solutions.

In the field of optical sensing and biomedical applications, mainly the potential for miniaturization and sensitivity improvement compared to state-of-the-art systems

adds to the attractiveness of integrated photonic solutions [14, 15]. Nowadays, waveguide-based optical sensors reach the detection limit of  $10^{-7}$ /refractive index unit (RIU) [14], which covers most interesting applications. Current research focuses on creating sensor arrays and cost price reduction by further miniaturization [16]. Recent progress in miniaturization of spectrometers for Raman detection and optical coherence tomography (OCT) [17–19] demonstrates the potential of photonics technology for point-of-care diagnostics. The requirements and technology needs for these application fields are, however, hard to generalize. The applicable wavelengths, for example, cover the spectrum of light ranging from UV-VIS for environmental monitoring and absorption spectroscopy, from VIS to near-IR for clinical investigation techniques such as Raman spectroscopy and OCT, up to the mid-IR for gas sensing and space exploration (wavelength ranges based on astronomy division and sensor response division schemes as addressed in [20] and references therein). Adding active functions (light sources, detectors, switches, etc.), microfluidic components, and/or nonreciprocal elements such as circulators increases the functional and technological complexity beyond the integration of passive circuitry. Therefore, one of the main challenges remains to be the access to cost-efficient (hybrid) assembly and packaging techniques.

Materials and technologies applied in integrated optics research and development vary over a wide range, e.g., doped silica, polymers, silicon-on-insulator, III-V semiconductors, chalcogenides, lithium niobate and dielectric materials such as  $\text{Si}_3\text{N}_4$  or  $\text{Al}_2\text{O}_3$ . In Figure 1, a (non-exclusive) overview of known optical materials is given, showing their applicability as function of wavelength. Although many material systems have been successfully applied in some of the application fields, none of the technologies is capable to fulfill the complete set

of requirements for all photonic applications. Therefore, the integration of complementary technologies is often pursued.

At present, three technology platforms are commercially available in multi-project wafer (MPW) runs: the III-V InP technology, silicon photonics, and the TriPleX platform. Customers have access to a library containing basic building blocks, allowing complex functional designs. Several design houses [22, 23] support these platforms. Fabrication facilities for these platforms are available: InP [24–27], silicon (Si) photonics [28–30], TriPleX [31–33]. The key property performances of these technologies are summarized in Figure 2.

As indicated in Figure 2, the InP technology is applied in the full range of active functionalities yielding a large variety of photonic applications, such as laser (array)s, (fast) modulators, and detectors. Si-photonics and TriPleX are both silicon based and can, therefore, rely on CMOS-compatible fabrication technology enabling low-cost volume manufacturing [11]. Silicon photonics has combined its passive platform with significant progress in the realization of on-chip detectors and modulators. Most applications can be found in datacom [35]. TriPleX has focused on passive performance (i.e., no on-chip gain media or high-frequency tuning) with ultralow loss over a wide wavelength range including the visible range down to near UV. TriPleX is widely applied for microwave photonics, sensors, and visible light applications [36, 37].

For all three platforms, tight curvature of waveguide bends enabling cascading of multiple structures and reduction of optical footprint is mandatory. Therefore, a large refractive index contrast between waveguide core and cladding is needed. On the other hand, very efficient coupling to low-contrast optical fibers has to be accomplished implying completely opposite requirements on the index contrast of the channel waveguide. For the TriPleX

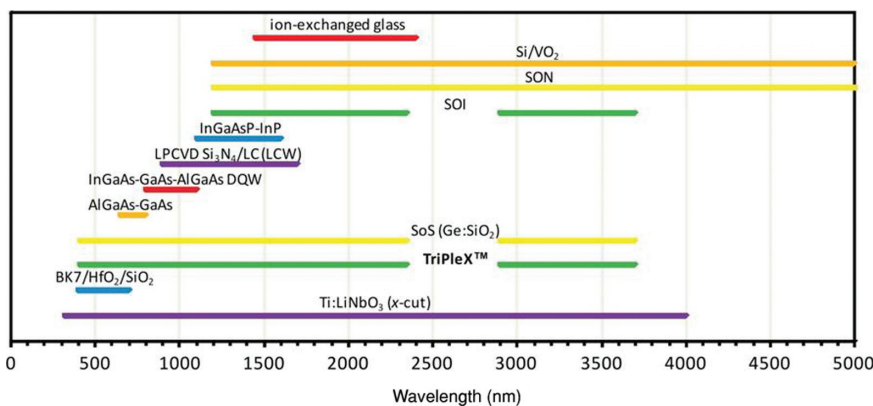


Figure 1: Overview on various materials applied in integrated optics and their corresponding transparency ranges [21].

Building block	Performance		
	InP	Si	TriPleX
Passive components	●	●●	●●●
Lasers	●●●	○	○
Modulators	●●●	●●	●
Switches	●●●	●●●	●
Optical amplifiers	●●●	○	○
Detectors	●●●	●●●	○

Performance	
●●●	Very good
●●	Good
●	Modest
○	Challenging

Footprint	●●	●●●	●
Chip cost	●	●●	●●
CMOS compatibility	○○	●●	●
Low-cost packaging	○	○ <sup>1</sup> /●● <sup>2</sup>	●●

**Figure 2:** Qualitative performance comparison of the three commercially available technology platforms [34].

platform, a monolithic spotsizer technology has been developed. This technology allows for on-chip modal field size conversion and, therefore, enables highly efficient fiber-to-chip coupling over the full accessible wavelength range while maintaining a large flexibility in waveguide geometry being inherent to the TriPleX photonic platform.

In this paper, we provide a comprehensive review on the TriPleX photonic waveguide platform. In Section 2, the properties, technological and design aspects will be discussed with emphasis on the different commercialized TriPleX geometries, integration aspects, fabrication concepts, and basic building blocks. Section 3 will focus on the applications and performance of TriPleX-based components for communications, biomedicine, and sensing as well as a few special fields of photonics.

## 2 TriPleX photonic platform

### 2.1 TriPleX technology and design

TriPleX waveguide technology is based on alternating well-defined and highly stable silicon oxide ( $\text{SiO}_2$ ) and silicon nitride ( $\text{Si}_3\text{N}_4$ ) layers [38, 39]. The CMOS-compatible fabrication equipment based on batch processing by low-pressure chemical vapor deposition (LPCVD) enables volume production as well as good reproducibility [32, 40]. TriPleX waveguides are transparent for wavelengths from 0.4 up to 2.35  $\mu\text{m}$  and exhibit very low optical propagation losses. This technology combines good integration potential with high design flexibility allowing for tailoring of the waveguide properties [41]. We distinguish three

commercially available basic waveguide geometries, which can be obtained by modification of individual steps in the generic fabrication flow [42]. The geometries are categorized by their shape: box shell (I), double stripe (II), and filled box (III), whereas type II is subdivided into the symmetric double stripe (IIa), the asymmetric double stripe (IIc), and the single stripe (IIb) being a special case of IIc. The schematic layouts of the geometries and SEM micrographs of realized structures are depicted in Figure 3. The generic process flow covering the fabrication steps of all TriPleX types is given in Figure 4.

While the overall geometrical dimensions of the waveguide cores of these shapes are typically in the order of  $1 \mu\text{m}^2$ , their waveguide characteristics and potential application areas differ greatly. Some key characteristics are effective index of the waveguide mode  $N_{\text{eff}}$  and group index  $N_g$  (for TE-polarized light), channel propagation loss  $\alpha_{\text{ch}}$  [dB/cm], polarization-dependent loss  $PDL$  [dB], minimum bending radius  $R_b$  [ $\mu\text{m}$ ], mode field diameter  $MFD$  [ $\mu\text{m}$ ] ( $\text{TE}_{00}$  mode), fiber-chip coupling loss  $\alpha_{\text{fc}}$  [dB/facet], and waveguide birefringence  $\Delta N_{\text{eff}}$ .

The *box shell* layout is highly suited for telecom applications: due to its symmetrical shape, the polarization dependence is largely reduced [43]. The box shell is available in a low [39] and high [44] index contrast variant based on different ratios of the  $\text{Si}_3\text{N}_4$  and  $\text{SiO}_2$  thicknesses in the core region. In the low contrast version, a  $1 \times 1 \mu\text{m}^2$   $\text{SiO}_2$  core is surrounded by 50-nm-thick  $\text{Si}_3\text{N}_4$ , while the high contrast is achieved with  $\text{SiO}_2$  and  $\text{Si}_3\text{N}_4$  core dimensions of  $0.5 \times 0.5 \mu\text{m}^2$  and 170 nm, respectively. The waveguide propagation loss of the high-contrast box shell geometry is below 0.2 dB/cm and reduces to 0.06 dB/cm for the low-contrast variant [45]. The main difference in the characteristics of both versions can be found in the bending

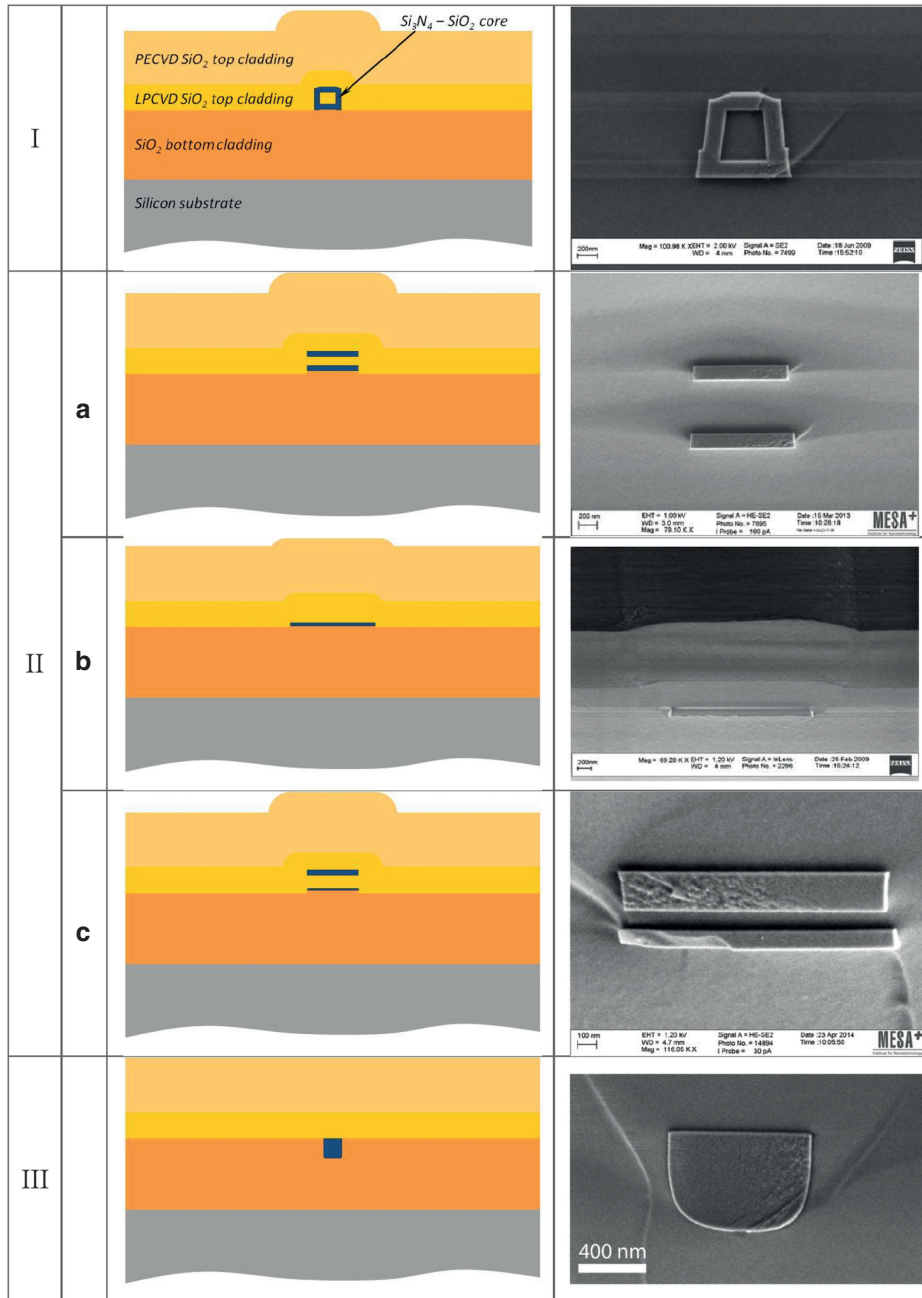


**Figure 3:** Schematic layout of the TriPleX geometries and SEM images of realized structures: box shell (I), symmetric double-strip (IIa), single stripe (IIb), a-symmetric double stripe (IIc), filled box (III).

radius, which is designed to fulfill the 0.01 dB/cm bend loss criterion, and the mode field diameter of the circular mode shape:  $R_b=500\ \mu\text{m}$ ,  $MFD=3.6\ \mu\text{m}$  (low contrast), and  $R_b=150\ \mu\text{m}$ ,  $MFD=1.4\ \mu\text{m}$  (high contrast).

The *symmetric double stripe* layout is typically applied in components requiring tight bending radii and large polarization birefringence. The optimized geometry is composed of two 170-nm-thick and 1.2- $\mu\text{m}$ -wide  $\text{Si}_3\text{N}_4$  layers separated by a 500-nm-thick  $\text{SiO}_2$  interlayer. The effective index of the waveguide mode at 1.55  $\mu\text{m}$

wavelength and the group index are 1.535 and 1.72, respectively, while the waveguide birefringence is  $5.3 \times 10^{-2}$ . The waveguide attenuation is  $\leq 0.1\ \text{dB/cm}$  [46]. The tight bending radius allows for functional complexity at VLSI level. As shown in Figure 5, waveguide propagation loss as low as 0.095 dB/cm was measured in optical ring resonator (ORR) structures with a bending radius down to 70  $\mu\text{m}$  [46]. The circular mode of this waveguide geometry has a mode field diameter of  $\sim 1.5\ \mu\text{m}$ . To enable low-loss coupling to standard single-mode fibers (SMF28),

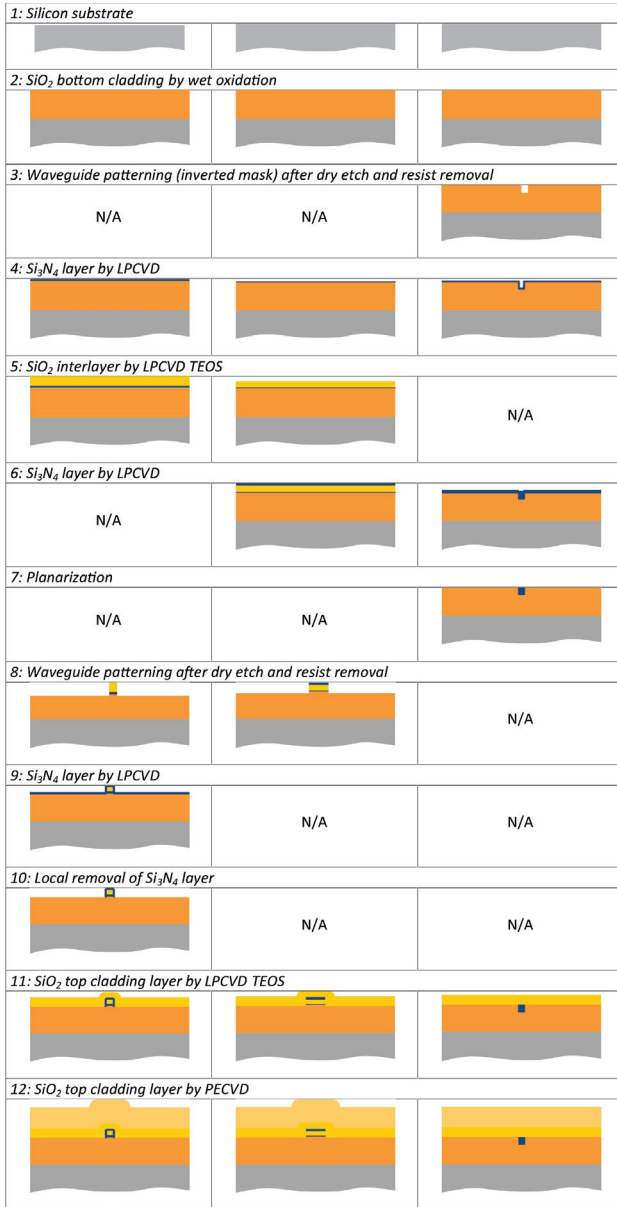


**Figure 4:** Generic process flow for the fabrication of the three basic TriPleX geometries.

both  $\text{Si}_3\text{N}_4$  stripes are adiabatically tapered in the vertical direction. The adiabaticity criterion is fulfilled if the angle of the MFD change is below  $1^\circ$  (i.e., geometrical taper angle  $\leq 0.01^\circ$ ). In case of this TriPleX geometry, this results in typical taper lengths of  $600\ \mu\text{m}$ . At an optimized thickness of  $35\ \text{nm}$  for both tapered  $\text{Si}_3\text{N}_4$  layers, fiber-chip coupling losses of  $<0.5\ \text{dB}$  were demonstrated.

The *a-symmetric double-stripe* geometry is highly suitable for combining regions with low and high effective indices of the mode on a single chip. In a realized example of this geometry type, a  $40\text{-nm}$ -thick low-contrast  $\text{Si}_3\text{N}_4$  stripe is separated in the vertical direction by a  $100\text{-nm}$

$\text{SiO}_2$  interlayer from the  $175\text{-nm}$ -thick high-contrast  $\text{Si}_3\text{N}_4$  channel [47]. An adiabatic transition is made between both contrast regions by tapering the thicker layer to zero. In the high-contrast region, the channel width is set to  $1.5\ \mu\text{m}$ , while the width in the low contrast area is variable. The high contrast waveguide exhibits an MFD of  $1.7\ \mu\text{m}$  and  $1.3\ \mu\text{m}$  in the in-plane and out-of-plane directions, respectively. The waveguide birefringence is in the order of  $5 \times 10^{-2}$ . Demonstrated loss values for the low and high modal confinement areas on the same chip were  $0.015\ \text{dB/cm}$  and  $0.15\ \text{dB/cm}$ , respectively.

The *single stripe* geometry is applied when extremely low optical losses are required: as explained, the single stripe can be converted from the asymmetric double stripe by locally removing the high-contrast waveguide. A detailed study on propagation loss and bending radii as a function of core aspect ratio (width/thickness) of this low-contrast stripe was carried out over a wide range of layer thicknesses ( $20\text{--}100\ \text{nm}$ ) and channel widths ( $0.3\text{--}14\ \mu\text{m}$ ) [48]. While high aspect ratios (channel width over thickness) are favorable for low propagation losses, the bending radius decreases at lower aspect ratios. Propagation losses as low as  $0.03\ \text{dB/cm}$  in a stripe geometry allowing for  $2\text{-mm}$  bending radii were demonstrated upon light propagation at  $1.5\ \mu\text{m}$  wavelength. Analyzing measured loss values with models taking into account various loss mechanisms the stripe propagation losses could be attributed to residual roughness and layer imperfections originating from the fabrication processes. The waveguide birefringence of  $100\text{-nm}$ -thick  $\text{Si}_3\text{N}_4$  waveguides with channel widths varying from  $1.4$  to  $3.5\ \mu\text{m}$  was investigated [49]. For core widths above  $2\ \mu\text{m}$ , the birefringence exceeds  $10^{-2}$  and good polarization-maintaining performance can, therefore, be expected. TE-pass polarizers with cross-polarization as low as  $-75\ \text{dB}$  (measurement limited) have been reported [50].

Significant improvement of the loss figure was achieved by optimization of the channel fabrication process and replacement of the upper PECVD  $\text{SiO}_2$  cladding layer by a bonded thermal  $\text{SiO}_2$  film [51]. The propagation loss through a single mode waveguide channel with  $50\text{-nm} \times 5.3\text{-}\mu\text{m}$  geometrical cross-section was reduced to  $0.007\ \text{dB/cm}$  [52]. Record-low loss of below  $0.0005\ \text{dB/cm}$  was measured at  $1.58\ \mu\text{m}$  wavelength on  $40\text{-nm} \times 13\text{-}\mu\text{m}$  and  $50\text{-nm} \times 6.5\text{-}\mu\text{m}$  multimode stripe waveguides [51].

The challenge of minimizing the bend radius while maintaining low propagation losses was addressed by various approaches. In Figure 6, light propagation through a stripe geometry based on  $40\text{-nm}$ -thick and  $14\text{-}\mu\text{m}$ -wide  $\text{Si}_3\text{N}_4$  core is demonstrated down to a bending radius of  $165\ \mu\text{m}$ . However, in that geometrical range, the channel is

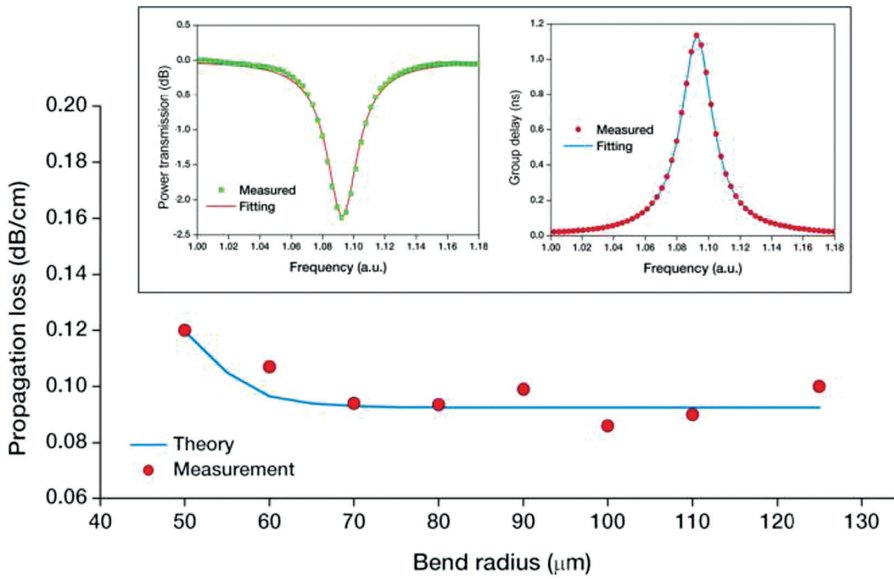


Figure 5: Waveguide propagation loss as function of ORR bending radius (inset: measurement and fit of ORR frequency responses) [46].

multimode, and an additional tapering section is required for adiabatic widening of the channel width [51].

Finally, the *filled-box* geometry was developed for applications requiring ultrahigh confinement of the modal field in the core layer. In this geometry, core widths of 0.8–1.0  $\mu\text{m}$  and thicknesses varying from 0.8 to 1.2  $\mu\text{m}$  were realized [53]. The waveguide channel is multimodal; up to three modes exist. For the 1.55- $\mu\text{m}$  wavelength and TE-polarized light, the corresponding effective index of the mode and MFD of the fundamental mode ( $\text{TE}_{00}$ ) are around 1.79 and 1  $\mu\text{m}$ , respectively. A minimum bending radius of 12.5  $\mu\text{m}$  was calculated for the  $\text{TE}_{00}$  mode taking the 0.01 dB/cm loss criterion into account. As stoichiometric LPCVD  $\text{Si}_3\text{N}_4$  films exhibit high tensile stress, the layer thickness growth is limited to <500 nm. Therefore,

trench etching (into the thermal oxide layer) and trench filling (by LPCVD  $\text{Si}_3\text{N}_4$  deposition) in combination with chemical mechanical polishing (CMP) was applied for the fabrication of crack-free waveguides (see also Figure 4). The optical propagation loss of these waveguides at 1.55  $\mu\text{m}$  wavelength was 0.4 dB/cm [53].

## 2.2 Technology integration aspects

The high design flexibility provided by the TriPleX platform is prerequisite to boost photonic integration. The availability of low- and high-contrast regions on a single chip easily enables interposer functionality in photonic assemblies. The large freedom in pitch and spotsize conversion is, for example, utilized in low-loss connections between optical fiber arrays and high-confinement waveguide technologies such as InP or silicon on insulator (SOI) [54]. In return, active functionality (light generation, detection, and modulation) available on those platforms is efficiently joined with the TriPleX circuitry. Various complementary functionalities such as high-Q resonators, arrayed waveguide gratings, tunable delay lines, and devices for polarization control available in the ultralow loss silicon nitride waveguide technology and in silicon photonics are reviewed [55, 56]. On the SOI side among others, modules based on hybrid integration with the III-V InP technology and magneto-optical materials add to the functionality portfolio. The proposed integration concepts for silicon nitride waveguides with the silicon photonic platform are based on a hybrid bonding process

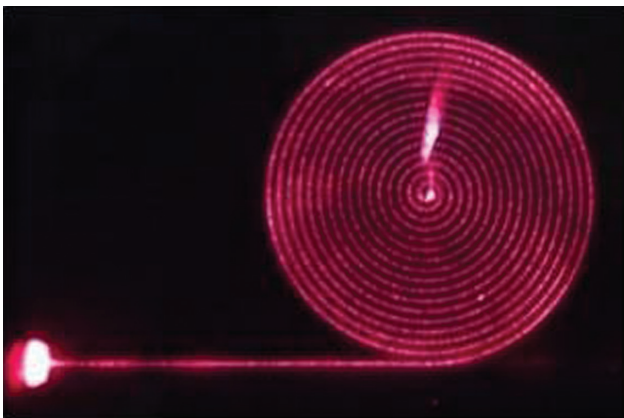


Figure 6: Red light propagation in a high-aspect ratio spiral-shaped waveguide with minimum bending radius of 165  $\mu\text{m}$  [51].

utilizing an  $\text{SiO}_2$  interface layer with a controlled thickness [57, 58]. The integration concept and an SEM micrograph of a fabricated device are shown in Figure 7.

Currently, a novel assembly concept for integrating InP and TriPleX chips on a carrier platform is being developed by a European consortium: PHASTFlex [59]. Besides addressing low-cost, high-volume assembly, the approach focuses on bridging the gap between typical flip-chip placement accuracies ( $\leq 1 \mu\text{m}$ ) and the sub-100-nm alignment precision required by high-contrast coupling interfaces by monolithically integrated MEMS-based fine tuning.

On-chip adiabatic tapering sections are key elements for many integration aspects. Therefore, the optimization of the taper design and technology was emphasized. Vertical tapers are usually fabricated by standard lithography and isotropic etching of the silicon nitride layers. Measurements of propagation losses through such tapering sections resulted in  $\leq 0.5 \text{ dB/taper}$  [47]. The most critical part of the tapering path is at the starting position of the taper (thin side), where the propagation of the weakly confined mode is extremely sensitive to geometrical changes. Therefore, LioniX has developed a novel ultrataper procedure, in which the shape of the tapering section can be

controlled by design rather than solely by the process-specific etch profile [60]. The preliminary results based on insertion loss measurements of waveguides with multiple tapering sections indicate a taper loss reduction by about one order of magnitude.

Last but not the least, the TriPleX platform is also well suited for lab-on-a-chip applications. Manufacturable concepts (Figure 8) for the integration of microfluidic systems as well as the assembly of VCSEL arrays and detectors have been developed [42, 61].

### 2.3 Technology access

Low-threshold access to the TriPleX platform is, among others, enabled through MPW services [62]. The MPW approach provides a solution for researchers and entrepreneurs to prototype their design at affordable cost and time levels. The designs of several participants are integrated on a single mask and fabricated in a shuttle run. Circuitry simulation and mask design can be carried out by Phoenix software tools [22]. A prerequisite to the successful implementation of such an approach is the availability of well-defined and verified design elements.

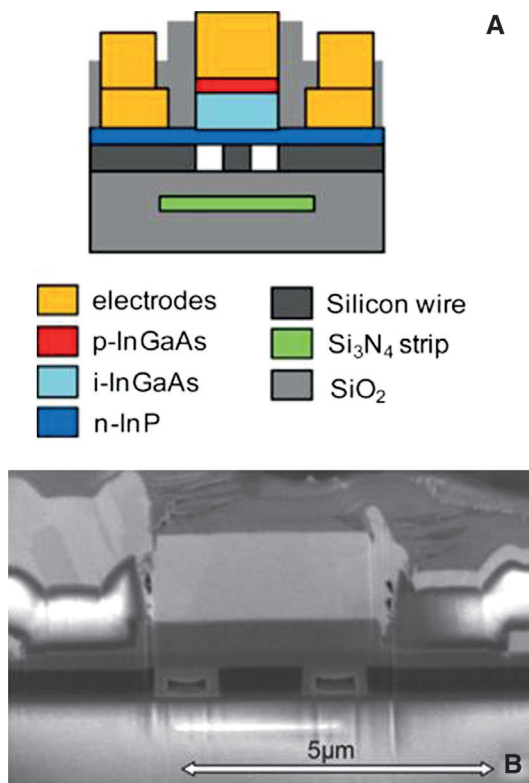


**Figure 7:** Concept of TriPleX integration with SOI and III/V: schematic view (A) and SEM micrograph of integration cross section (B) [57].

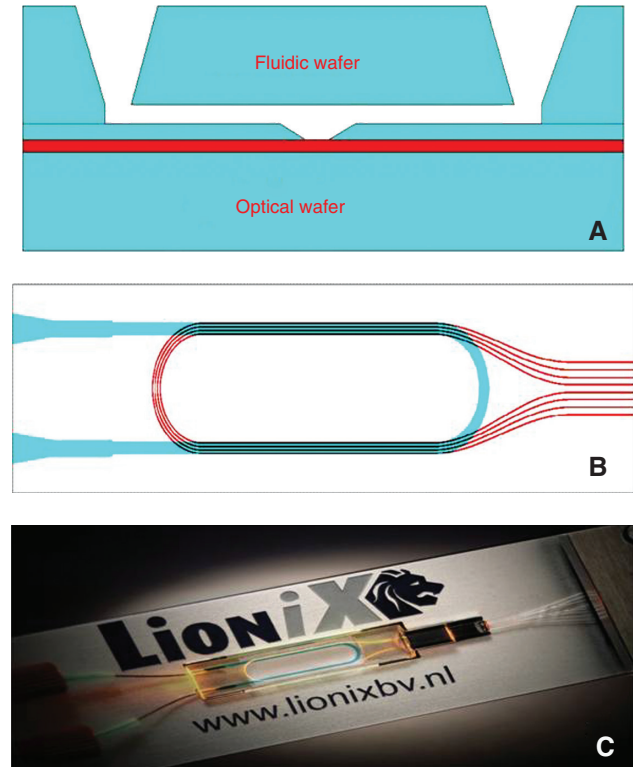


**Figure 8:** Concept of optofluidic assembly showing schematic of chip cross-section (A) and top view (B) as well as a picture of a component sub-assembly (C) [61].

Therefore, a library of standard optical components was established and implemented as basic building blocks (BBBs) in the licensed design kit of the PhoeniX software. In the past MPW services, components for the box shell geometry were applied, while in currently active MPW calls, the double-stripe geometry is offered. The BBB libraries include the following main elements: waveguide straight, bent waveguide, Y-junction, directional coupler, spotsizer converter, and heater section. This allows for the easy design of integrated functions such as interposers, microring resonators (MRRs), several types of interferometers (multimode, Michelson, Young, Mach-Zehnder), arrayed waveguide gratings, multiplexers, frequency, and modal filters, mode and polarization converters as well as implementation of thermo-optic tuning or sensing windows. The library kit for the asymmetric stripe geometry is under preparation.

TriPleX services as well as its combination with other photonic platforms and technologies are also available through the European initiative ACTPHAST [63], which has created a unique *one-stop-shop* European access center for photonics innovation solutions and technology support.

### 3 Application fields

In this section, we will review the performance of TriPleX photonics technology reported for a wide range of application fields. Several components for communications will be addressed first. Then details on state of the art in biomedical and sensing applications will be given, followed by several special areas such as nonlinear optics, light generation, and components for space.

#### 3.1 Communications

In many cases, photonic functions used in communication applications like true time delay networks, wavelength routing, data packet buffering, narrowband filtering, timing references, or narrow linewidth light sources are based on long propagation distances or resonators with high-quality factor and require, therefore, extremely low propagation loss ( $<0.10$  dB/cm) [47]. A range of TriPleX-based photonic functions and building blocks applicable in telecommunication components including integration with the III-V or silicon platforms was recently investigated by researchers of UCSB [55].

State-of-the-art quality factors exceeding  $4 \times 10^8$  have been demonstrated in silica microtoroids on a chip [64].

Light coupling to the toroidal cavities is usually realized through tapered fibers because on-chip integration of access waveguides is challenging. The integration of high-Q ring resonators in the ultralow-loss TriPleX platform is an attractive approach, as access waveguides, cavities, and directional couplers can be monolithically integrated. In the TriPleX single stripe geometry ( $40 \text{ nm} \times 11 \text{ }\mu\text{m}$ ), add-drop ring resonators, with a 9.65-mm bending radius and a 3.3-GHz FSR at 1580 nm wavelength, have been integrated [65, 66]. Several directional coupler concepts (symmetric, straight, pulley, and tapered) have been implemented to assess and minimize the coupler excess loss. An intrinsic Q-factor of  $0.81 \times 10^8$  was measured with a weakly tapered directional coupler design. Round trip and propagation losses of 0.019 dB and 0.0032 dB/cm were extracted, respectively. Upon further coupler optimization and full exploitation of the low-loss TriPleX platform (i.e.,  $\alpha_{ch} < 0.0005$  dB/cm) Q-factors as high as  $6 \times 10^8$  are predicted.

A range of ring resonators suited for application over a wide wavelength range (1060, 1310 and 1550 nm) was studied in [67]. Based on single-mode TE propagation in two different TriPleX single stripe geometries ( $50 \text{ nm} \times 5.3 \text{ }\mu\text{m}$  and  $80 \text{ nm} \times 2.8 \text{ }\mu\text{m}$  with bending radii of 5 and 2 mm, respectively), Q-factors of 19, 28,  $7 \times 10^6$  were demonstrated at 1060, 1310, and 1550 nm wavelength, respectively. Analysis of the filter characteristics resulted in 16, 38, 300 MHz bandwidths for the 1060, 1310, and 1550 nm operations, respectively. The performance, as well as the wide wavelength range, makes these building blocks attractive for many applications ranging from ultranarrowband MWP filters to highly sensitive biosensors.

For the integration (de)multiplexing functionality in the 1310- and 1550-nm wavelength ranges, 16-channel arrayed waveguide gratings (AWG) with a 200-GHz channel spacing were realized in TriPleX single stripe geometry ( $50 \text{ nm} \times 5.5 \text{ }\mu\text{m}$ ) on a chip footprint of  $15 \text{ mm} \times 20 \text{ mm}$  [68]. The component layout is depicted in Figure 9A. For an operation at  $1.3 \text{ }\mu\text{m}$  wavelength, an FSR of 18.8 nm (2350 GHz), adjacent channel crosstalk of -30 dB and non-adjacent channel crosstalk of -40 dB were measured. The measured performance of the AWG in the  $1.5\text{-}\mu\text{m}$  wavelengths range is shown in Figure 9B. Furthermore, the spectral response to a change in temperature ( $\Delta\lambda/\Delta T$ ) was measured to be  $1.1 \times 10^{-2}$  nm/ $^\circ\text{C}$ . The implementation of AWGs in a 400-Gb/s WDM receiver unit with hybrid integrated detectors was demonstrated as well [58].

Another highly interesting area in communications is MWP being an interdisciplinary field investigating the techniques for generation, transmission, processing, and analyzing of RF/microwave signals using photonic devices

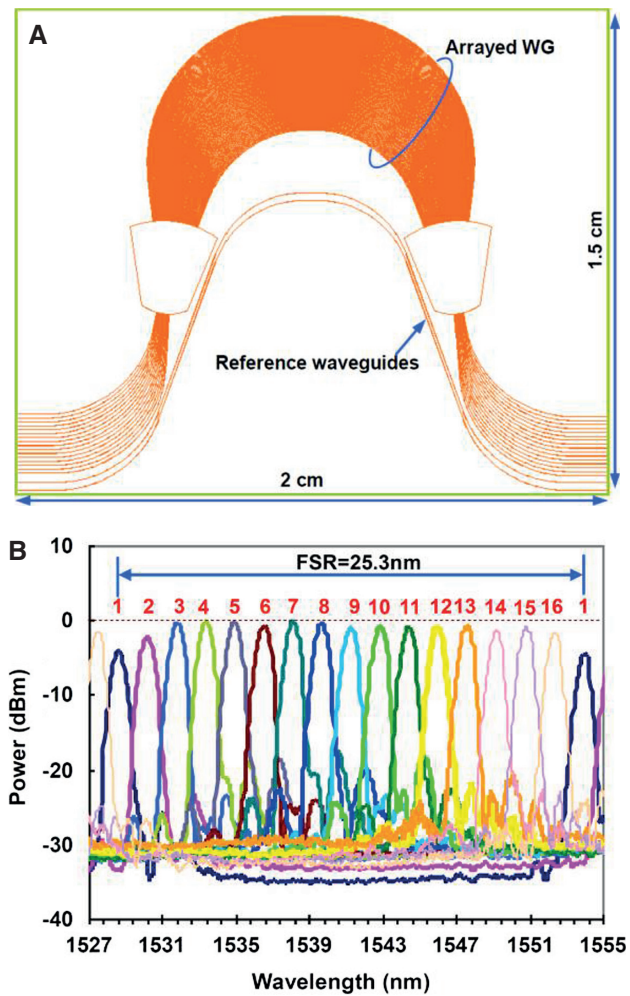


**Figure 9:** Schematic layout of AWG component (A) and measured characteristic of 16-channel AWG realized in TriPleX geometry (B) [68].

or subsystems [7]. The properties of photonic components, such as large instantaneous bandwidth, low loss, small size and weight, immunity from electromagnetic interference (EMI), as well as easy tunability and reconfigurability, are leveraged to realize novel RF/microwave functionalities with unprecedented features [8].

In recent years, a number of RF/microwave functionalities have been demonstrated using on-chip MWP signal processing in TriPleX technology. Examples range from tunable microwave filters, phase shifters, frequency converters, ultra-wideband microwave signal generators to tunable true time delay (TTD) elements for optical beam-forming networks (OBFN) [69–73]. A detailed discussion of the basic building blocks applied in integrated OBFNs can be found in [33].

The optical components are based on optical MRRs. Tuning and bandwidth reconfiguration in the order of a few GHz can be easily implemented, and squint-free

performance and seamless beam steering for broadband applications are enabled. For the utilization of OBFNs in satellite-tracking phased array antenna system operating in the  $K_u$ -band (10.7–12.75 GHz) delay lengths in the order of tens of centimeter are required. Consequently, low loss and compact waveguide configurations are essential for meeting performance and cost requirements. Therefore, the double stripe TriPleX geometry enabling MRRs with 125  $\mu\text{m}$  radius is chosen.

To date, three different types of optical beam formers have been implemented with our technology: single wavelength, multi-wavelength, and multi-beam [74]. A realized chip of a  $16 \times 1$  single wavelength OBFN component is shown in Figure 10A. On the  $7\text{-mm} \times 22\text{-mm}$  chip area, a TTD unit with 40 MRRs, splitters/combiners, and an optical sideband filter are included [33, 76]. Delays of 650 ps over a 4.5-GHz bandwidth were measured.

By introducing a novel hardware architecture [75] based on parallelism, a  $16 \times 16$  multi-wavelength OBFN could be realized on chip real estate as small as  $36 \times 8 \text{ mm}^2$ . Besides

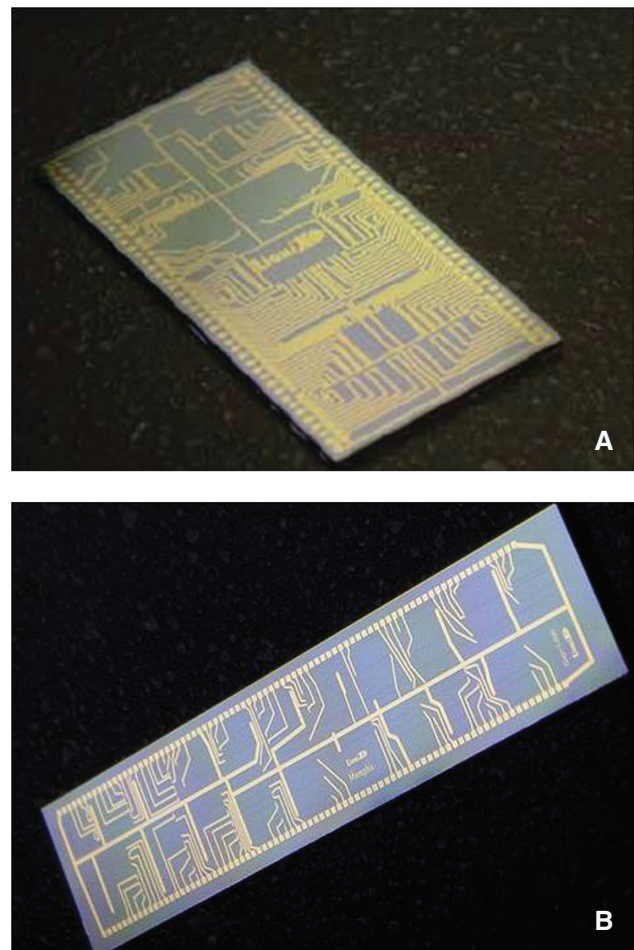


**Figure 10:** Pictures of  $16 \times 1$  single wavelength OBFN chip [8] (A) and  $16 \times 16$  multi-wavelength OBFN chip [75] (B).

delay units and combiners, this chip (Figure 10B) contains optical phase shifters, carrier tuners, and (de)multiplexers. A continuously tunable delay of up to 140 ps was measured over an instantaneous bandwidth from 2 to 10 GHz.

A multi-beam layout based on a Nolen matrix has gone through the design phase. For a 255-antenna $\times$ 36-beam Nolen matrix based on tunable Mach-Zehnder coupler unit cells, a chip size around 90 cm<sup>2</sup> is expected. This footprint represents a reduction of three orders of magnitude compared to conventional RF-BFN techniques [74].

A fully packaged optical TTD component for wide bandwidth signals and an insertion loss of 5.3 dB was reported by Morton et al. [77, 78]. Delays of 535 ps and 632 ps were measured for 10 and 20 GHz wide signals, respectively.

Another approach for integrated 4-bit tunable temporal delay lines has been demonstrated by switching spiral-shaped waveguides based on the single stripe TriPleX geometry [79] over a chip area of 4.5 $\times$ 8.5 cm<sup>2</sup>. Delays of up to 12.35 ns with 0.85 ns resolution were measured. The insertion loss measured for all 16 states varied from -12 to -14 dB.

Further developments toward a fully integrated and low-cost MWP beamformer system exploit the large-scale integration potential of the TriPleX technology. Simultaneous implementation of components operating with phase modulation and direct detection [80] is reported, and novel fully tunable RF filters are implemented [81]. The various stages of the MPW beamformer system – from the filter schematic to the fully packaged commercial product – are depicted in Figure 11A–D.

### 3.2 Biophotonics

As mentioned Section 1, integrated photonics solutions become increasingly important for biomedical applications and started to enter fields like OCT, Raman spectroscopy, flow cytometry, etc. TriPleX-based photonics technology has been applied for a range of novel, miniaturized biomedical components.

Optical coherence tomography (OCT) is a widely applied noninvasive medical imaging technique for 3-D biological tissue investigation. The technique is based on low-coherence interferometry from scattering media. Operation in the 800- to 1300-nm wavelength range enables up to several millimeter penetration depth in the tissue. Utilization of wide spectral ranges (>100 nm) result in submicrometer resolution. In spectral domain OCT, we distinguish two basic data acquisition modes: swept-source and spectrometer-based OCT.

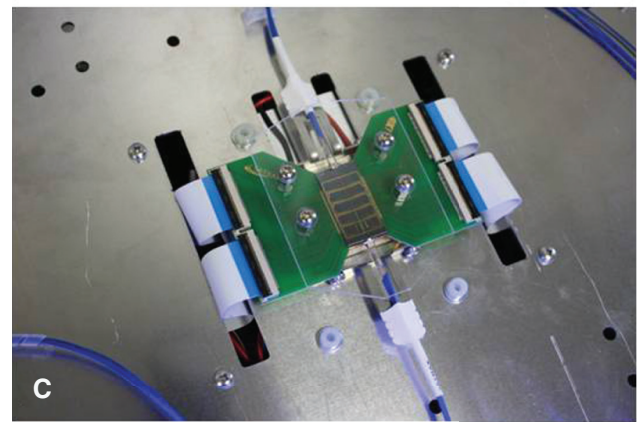
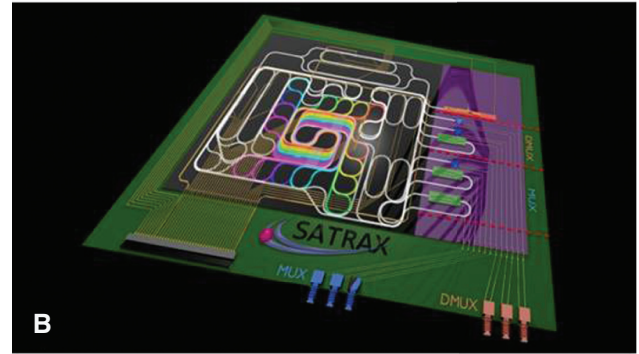
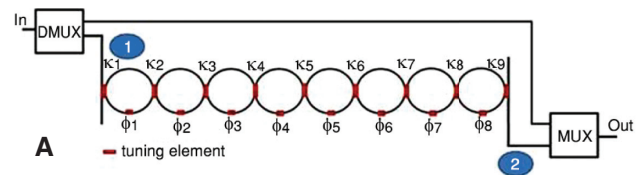


**Figure 11:** Schematic of fully tunable rf filter [81] (A), artist impression of chip layout on circuit board (B), fabricated chip assembly (C), and operational commercial product (courtesy SatraX) (D).

An integrated design for swept-source OCT operating with an external swept source at 1300 nm was developed in cooperation with the AMC in Amsterdam (Figure 12) [82]. The TriPleX chip functionality is designed in single-stripe TriPleX geometry (50 nm $\times$ 3.4  $\mu$ m) and has a chip

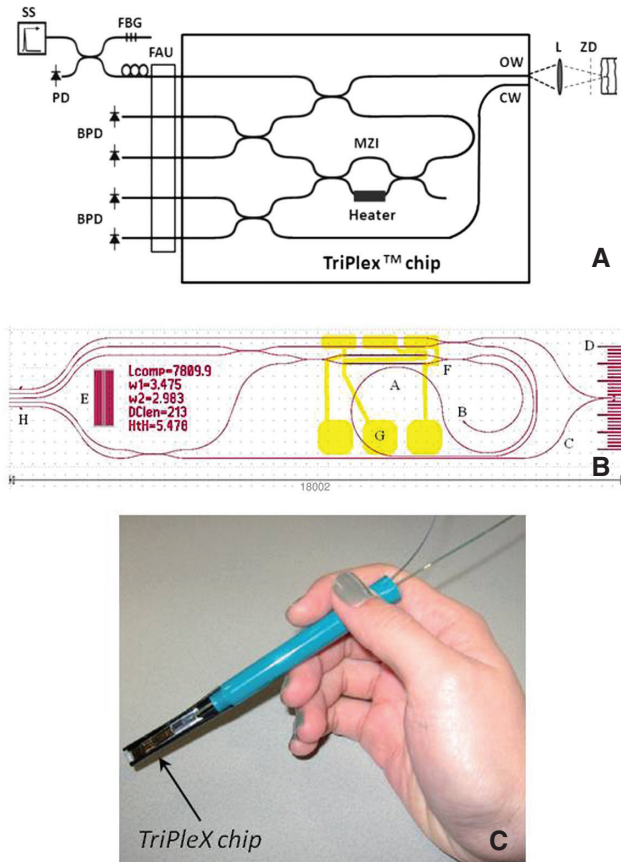


**Figure 12:** Schematic layout of swept-source OCT setup [82] (A), design of TriPLeX chip layout (B), and example of handheld component (courtesy 2M) (C).

footprint of  $4\text{ mm} \times 18\text{ mm}$  (Figure 12B). Component characterization resulted in  $21 \pm 1\ \mu\text{m}$  lateral resolution,  $-80\text{ dB}$  sensitivity, and a maximum imaging depth of  $5.09\text{ mm}$ . The axial resolution of  $12.7 \pm 0.5\ \mu\text{m}$  is in agreement with the bandwidth-limited resolution.

Exploiting the TriPLeX box shell geometry, an integrated interferometer chip for spectrometer-based OCT was developed by Ghent University in one of the MPW runs [45]. The design supports both polarizations and combines several Y-branches with a  $190\text{-mm}$ -long reference arm at a footprint of only  $10\text{ mm} \times 33\text{ mm}$  (Figure 13). The axial resolution of the system was  $14\ \mu\text{m}$ . The sensitivity measured at  $0.25\text{ mm}$  depth and  $0.1\text{ mW}$  optical powers on the sample was  $65\text{ dB}$ . Comparison with the response of a fiber-based system showed good agreement in performance. As dispersion control is an important aspect in wide-range spectral systems, the reduction of group velocity dispersion is investigated, and its potential implementation devices based on TriPLeX geometry is discussed.

The integration of TriPLeX box shell geometry waveguides with microfluidic channels was applied in the demonstration of optical particle trapping in combination

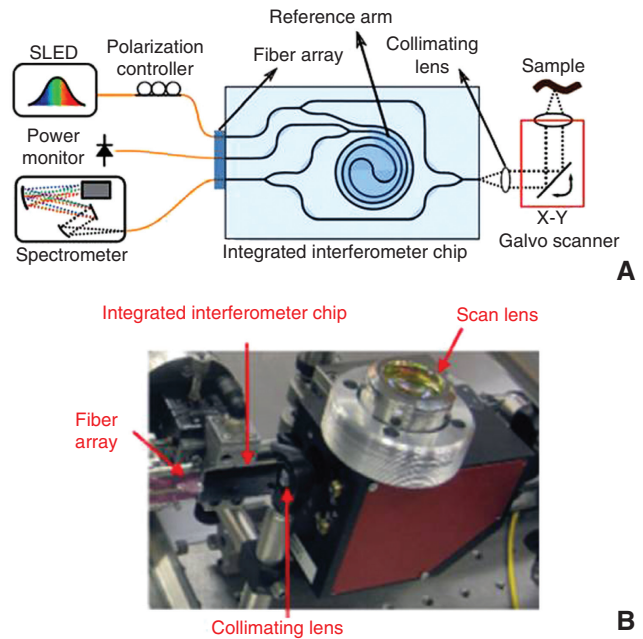


**Figure 13:** Schematic layout of the OCT setup with the integrated TriPLeX-based interferometer chip (A) and photograph of test setup with fiber array, integrated interferometer chip and scan lens (B) [45].

with Raman spectroscopy, which was realized in one of the MPW runs [83]. The optical trap was created by splitting the  $785\text{-nm}$  optical signal by a  $3\text{-dB}$  Y-junction over two excitation branches facing toward each other at the  $5\text{-}\mu\text{m}$ -wide trapping and excitation region of the fluidic channel (Figure 14). Chip dimensions were as small as  $8\text{ mm} \times 16\text{ mm}$ . Strong trapping forces as well as measurements of Raman spectra over integration times as short as  $0.25\text{ s}$  were demonstrated.

A highly useful component for many biomedical and sensing applications is an integrated optical version of a laser beam combiner (LBC). The component developed by XiO Photonics combines the emission from four to eight laser sources in the  $400\text{-}$  to  $850\text{-nm}$  wavelength range into one single-mode fiber output [37, 84]. On-chip polarization maintaining filtering functions based on o.a. MRRs in TriPLeX technology are applied. The resulting fully packaged component, as shown in Figure 15, is highly compact.

### 3.3 Optical sensing

Integrated optical circuits are increasingly applied for the detection of chemical and biological substances [85], as they enable high measurement resolution and high sensitivity over a wide dynamic range. Compact integration of relevant optical functions, such as mode filters and interferometers, can be realized at a low cost. TriPLeX

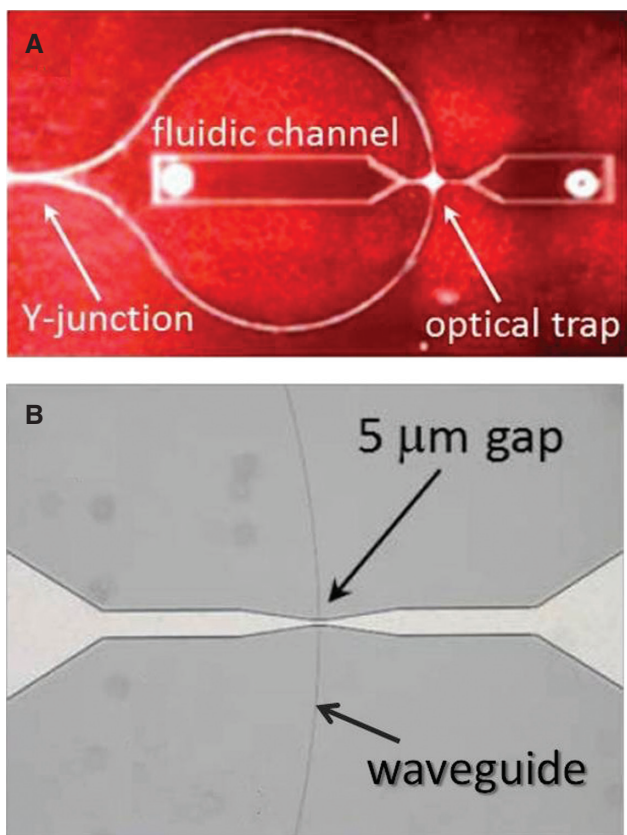


**Figure 14:** Microscope images of TriPleX chip for Raman spectroscopy on trapped particles upon coupling of red light (A) and of the trapping region of the device showing the microfluidic channel with the dual waveguide trap (B) [83].

technology can be applied over the relevant wavelength range of this application field and provides, moreover, a chemically stable detection platform [86].

**Sensing principle:** In these optical chips, the chemical parameter to be sensed (i.e., the measurand) influences the propagation properties of a guided light signal that propagates through an on-chip sensing region. The relevant interactions occur primarily in the evanescent field region just above the interface of the waveguide core layer, which can be accessed through a sensing window in the cover layer (see Figure 16). Generally, selectivity is provided by the chemo-optical transduction layer. This layer contains receptor units with selective affinity to the chemical entities of the measurand. Using identical optical chips and electronics, the concentration of a large variety of measurands can be determined by applying different transduction layers, such as antibody proteins as receptor molecules for immunosensors [87] or silicates containing functional organic groups for gas sensors [88]. We distinguish between refractive index, absorption, and fluorescence sensing.

**Refractive index sensing:** The sensor design can be either based on MRRs [89, 90] or on a Mach-Zehnder interferometer (MZI) [87, 91–93] configuration. The state of the art in MZI-based sensing platforms – being widely applied by LioniX’ customers – will be subject to future publication. In this review, we focus on the reported sensor performance based on the MRR approach.

The layout of the MRR component is based on a ring-shaped resonator waveguide with two directional couplers having a length  $L_{cd}$  and a gap  $g$ . For the design of the MRR sensor, the 850-nm wavelength is chosen enabling the use of low-cost VCSEL light sources. The MRR performance is optimized for the 100-nm-thick  $\text{Si}_3\text{N}_4$  single stripe waveguides previously shown to result in highly sensitive performance in evanescent wave sensing. Based on a waveguide channel width of 1.0  $\mu\text{m}$ , MRR with radii of 50 and 75  $\mu\text{m}$  are designed. For  $g=0.75 \mu\text{m}$  and  $L_{dc}$  varying from 0 to 250  $\mu\text{m}$ , FSR values ranging from 360 to 880 pm are feasible [42]. To realize low-loss coupling to the pigtailed VCSEL, spotsizes conversion is utilized by tapering the  $\text{Si}_3\text{N}_4$  thickness to 25 nm.

The schematic layout of the MRR sensor chip is illustrated in Figure 17A. The spotsizes conversion area with reduced waveguide thickness is indicated in green. The chip contains three MRRs, of which one serves as reference resonator (top cladding not removed), and two MRRs are equipped with a sensing window (indicated in blue). A microscope image of the fabricated chip is shown in Figure 17B. The response of a microring with a 50- $\mu\text{m}$  radius and  $L_{dc}=200 \mu\text{m}$  was measured with a tunable 850-nm VCSEL (Figure 17C). The measured FRS of 560 pm is in good agreement with the simulation results.

The lab-on-a-chip application potential of this sensor chip was investigated after integration with a microfluidic flow cell. Refractive index measurements in the fluidic channel resulted in a sensor response of  $110 \pm 22 \text{ nm/RIU}$  being an equivalent to a measurement resolution in the order of  $10^{-6}$  RIU. Label-free biochemical surface reactions have been demonstrated with bovine serum albumin (bSA). The response curve to bSA concentrations ranging from  $1 \times 10^{-7}$  to  $2.2 \times 10^{-4}$  M is shown in Figure 17D. Based on the theoretical biochemical surface sensitivity shift for bSA, the detection limit of our sensor was estimated to be smaller than 1 pm of an average bSA layer growth. The feasibility of gas sensing was shown in a preliminary experiment based on the interaction between acetone and a Teflon transduction film applied in the sensing window. A quick sensor response was observed upon the presence of acetone in a beaker being in the proximity of the sensor device.

The feasibility of multichannel sensing was assessed for an eightfold MRR array designed in the asymmetric

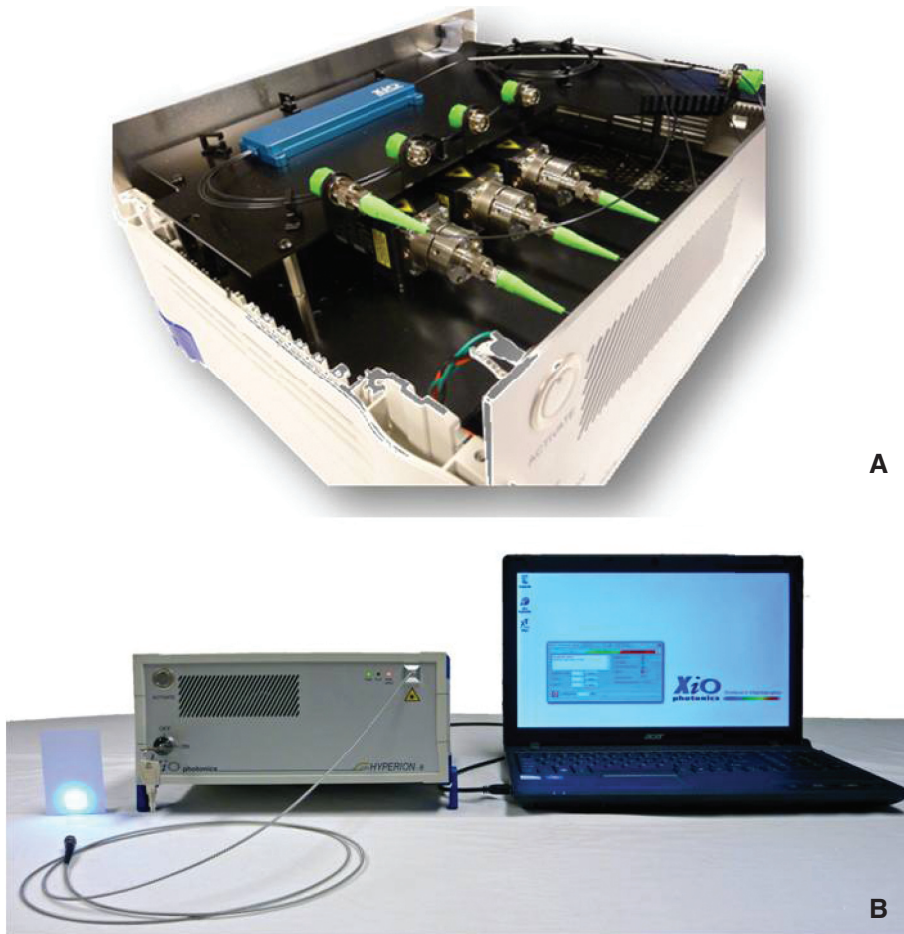


**Figure 15:** Photograph of Hyperion laser light engine [37]: modular interior with TriPleX LCB chip in blue pig-tailed package (A) and commercial product with software in action (courtesy XiO photonics) (B).

stripe TriPleX geometry with 35 nm and 85 nm lower and upper silicon nitride layer thickness, respectively [94]. Challenges with respect to power budget aspects in multichannel operations are addressed by a grating-based vertical VCSEL coupling concept in combination with an optimized  $1 \times 8$  multimode interference (MMI) coupler.

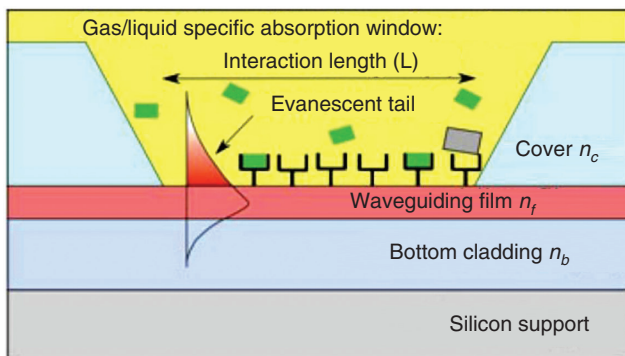


**Figure 16:** Sensing principle [42].

*Absorption sensing:* TriPleX-based chips have been designed and realized for a range of absorption-based applications in fluidic environments.

The development of processes in a microreactor largely benefits from integrated UV/VIS spectroscopic detection allowing for real-time analysis under segmented flow. An optofluidic chip optimized for evanescent field sensing based on a 65-nm-thick  $\text{Si}_3\text{N}_4$  waveguide layer and an operational wavelength range from 488 to 632 nm was developed for the monitoring of gold nanoparticle production [61]. Segmented flow detection at integration times as low as 2 ms was demonstrated.

*Fluorescence sensing:* A sensitive and low-cost detection scheme for molecular biomarkers has been demonstrated [95, 96] in TriPleX chips of  $10 \text{ mm} \times 10 \text{ mm}$ . One of the applied chip layouts yielding a matrix of 100 sensing wells is depicted in Figure 18. Light of 642-nm wavelength is coupled from a low-cost diode laser array into the excitation waveguides of the chip. In each sensing well, analyte molecules can be captured.

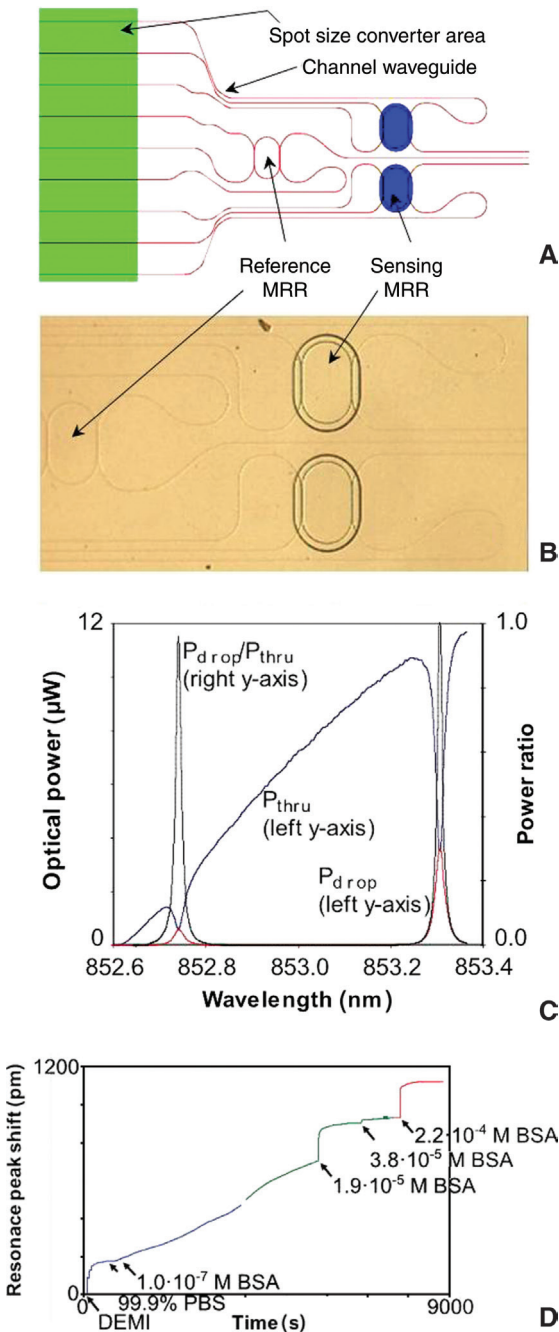


**Figure 17:** Schematic layout (A) and microscope picture (B) of MRR-based sensor chip. Measured MRR response (C) and resonance peak shifts upon application of bSA in various concentrations (D) [42].

Excitation of the analytes is realized in the sensing wells, where the excitation light penetrates to a depth of about 70 nm. Fluorescence emission from analyte molecules is back-coupled into the collection waveguide and measured by a detector array.

The main advantages of such a microarray-based approach can be found in short acquisition times (typically 5–10 min), very high sensitivity (1 fM or smaller), and

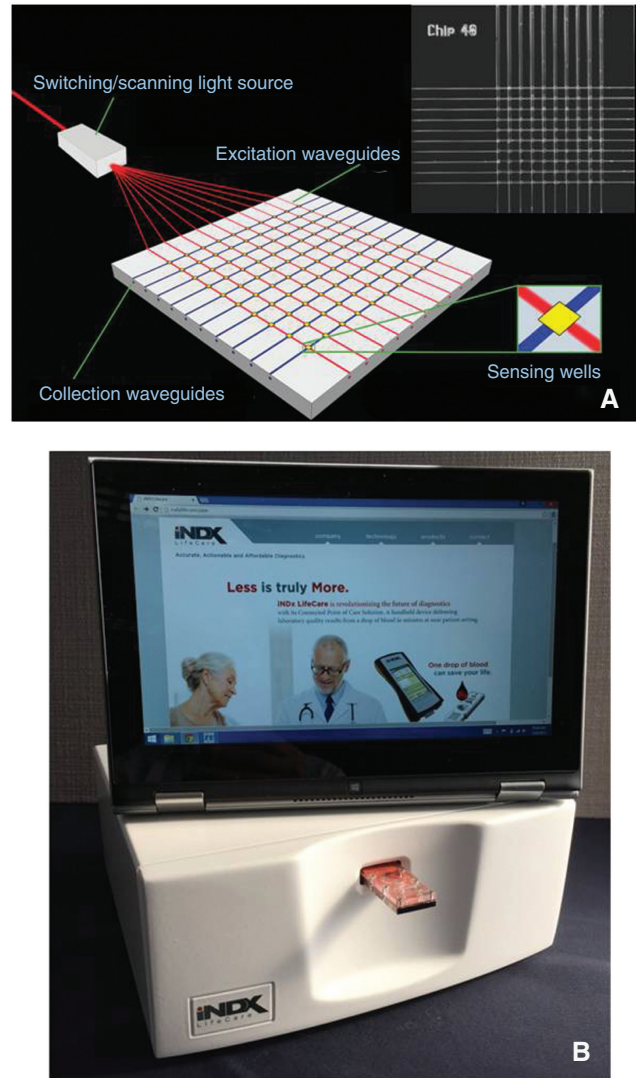


**Figure 18:** Schematic chip layout of fluorescence sensor array containing excitation waveguides, sensing wells, and collection waveguides (inset part: microscope image of fabricated chip) [96] (A) and operational commercial product with software (courtesy INDX Lifecare Inc.) (B).

applicability for multispecies sensing in complex matrices such as blood, whole serum, or urine. To the particularly interesting application fields belongs early stage cancer detection, screening for infectious diseases, or asymptomatic individuals testing following a biohazard event. Moreover, the systems fulfill requirements for point of care applications as they are low-cost, portable, battery operated, and allow for wireless connectivity.

For another customer, a multichannel fluorescence-based sensing system with a  $10 \times 10$  marker array for life detection on the ExoMars mission was developed [97]. The pigtailed module operating at 635 nm wavelength was realized in LioniX' optofluidic platform. Between the fiber input and the assay chamber containing the marker array,

the optical signal is split by a  $1\times 11$  MMI. The optical and fluidic modules are connected by a bonding process and diced to a chip size of  $52\text{ mm}\times 16\text{ mm}$ .

### 3.4 Special applications

Besides the above-discussed conventional application fields, the technology platform has also entered emerging areas of photonics and special applications such as integrated light sources, nonlinear optic devices, components for space, and quantum computing.

The active/passive integration potential of the silicon nitride technology was, for example, demonstrated by the monolithic implementation of optically pumped DFB lasers (Figure 19). For this purpose, side wall gratings with 520-nm period have been etched by stepper lithography into the  $4.6\text{-}\mu\text{m}$ -wide silicon nitride channel waveguides [98]. The grating coupling constant can be controlled between 13 and  $310\text{ cm}^{-1}$  by adjusting the aspect

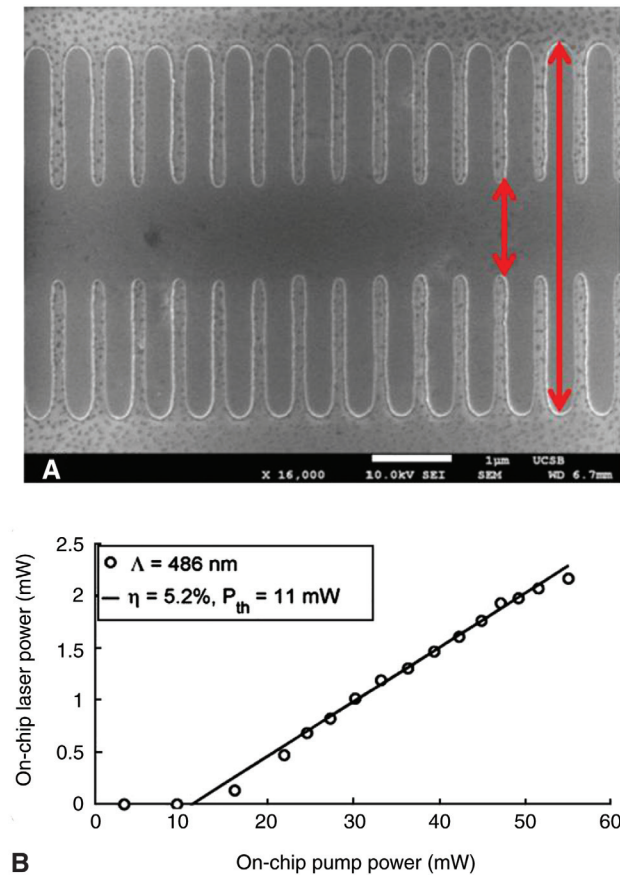


**Figure 19:** SEM image of sidewall gratings fabricated in  $\text{Si}_3\text{N}_4$  channel waveguide with red arrows indicating the channel-grating aspect ratio (A) and measured DBR laser output characteristic (B) [98, 99].

ratio between the original channel width and the sidewall gratings. High grating reflectivity was measured in the 1550-nm wavelength range. On top of the passive  $\text{Si}_3\text{N}_4$  platform an erbium ( $\text{Er}^{3+}$ )-doped aluminum oxide film with an  $\text{Er}^{3+}$  concentration of  $1.3\times 10^{20}\text{ cm}^{-3}$  was integrated by reactive co-sputtering [99]. The laser performance of several DBR and DFB grating configurations was measured applying 974-nm pumping. Pump thresholds, laser output powers, conversion efficiencies, and side mode suppressions of 11 mW, 2.1 mW, 5.2%, and 50dB, respectively, were achieved.

Ultra-narrow linewidth laser components have been realized by hybrid integration of III-V laser diodes with a TriPleX cavity in a so-called waveguide-based external cavity semiconductor laser (WECSL) configuration [100]. The design is based on the box shell geometry and exploits the response of two integrated MRRs acting as external mirror and having radii of 50 and  $55\text{ }\mu\text{m}$ , respectively. The layout of the frequency-selective mirror component realized in TriPleX technology is shown in Figure 20. A laser diode equipped with only one mirror is connected to the input port (IN) of the chip. To monitor the laser and mirror performance in greater detail, three output ports (OUT) are added to the design, whereas OUT3 provides the actual response of the WECSL. The measured FWHM laser linewidth and side mode suppression ratio of the WECSL are 25 kHz and 50 dB, respectively. Wavelength tuning over the full telecommunications C-band (1530–1565 nm) is demonstrated.

For nonlinear optic applications, high modal confinement in the photonic waveguide is of importance. Therefore, the filled box geometry of the TriPleX platform with core cross sections of  $1.2\text{ }\mu\text{m}\times 0.8\text{ }\mu\text{m}$  is highly attractive. In ongoing research, this technology is implemented for the design and realization of components for supercontinuum generation with over 700 nm spectral bandwidth [101] and four-wave mixing in the 800–1500 nm wavelength range [102].

The specific requirements of several applications for space research can be met by the TriPleX technology.

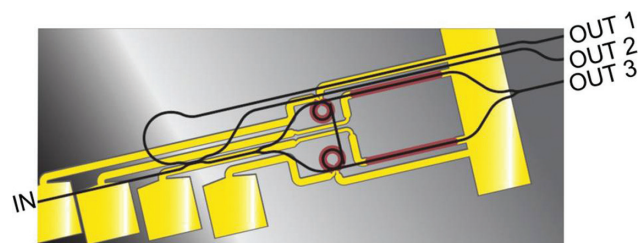


**Figure 20:** Schematic layout of the TriPleX waveguide chip showing the splitter, coupler and MRR configuration as well as the heater elements [100].

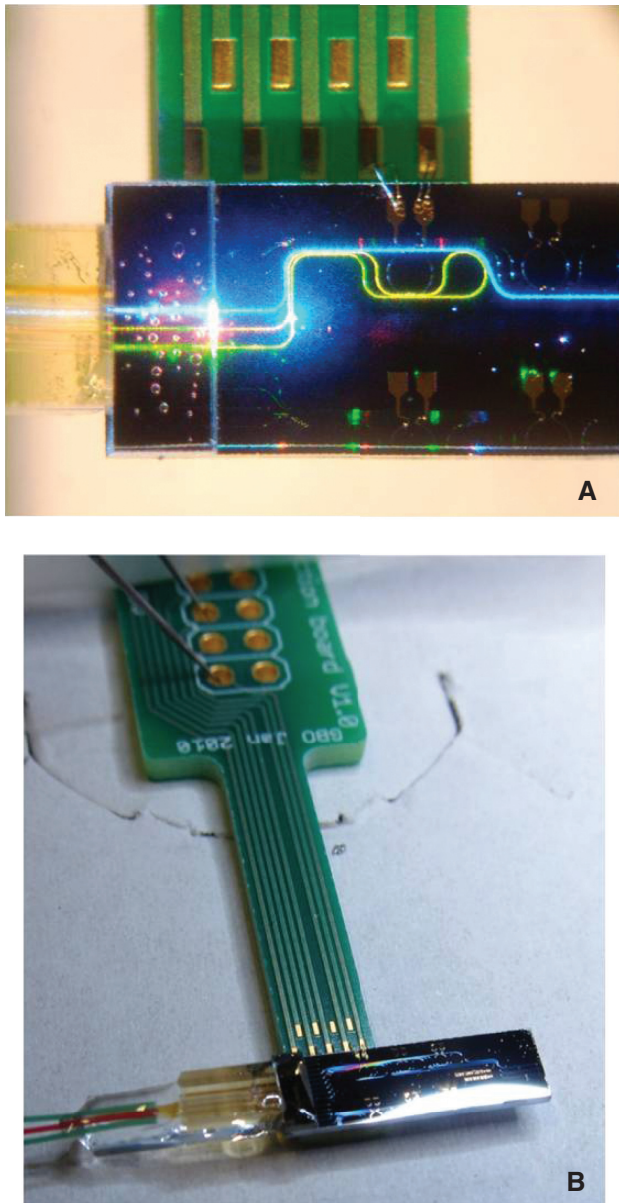


**Figure 21:** MRR-based in-flight calibration module for earth-orbiting satellites; optical chip propagation inspection with VIS light (A) and module assembly (B) [21].

In general, components for space missions need to be highly compact, robust, lightweight, and low on power consumption. One example of a realized module for the ExoMars mission was discussed in the fluorescence sensing section of this paper. Another application is addressed by the development of spectroscopic techniques on earth-orbiting satellites where an in-flight calibration module for the 2.3- to 2.4- $\mu\text{m}$  wavelength range was designed with thermally tunable MRR building blocks based on the asymmetric stripe geometry [21, 103]. The packaged module (Figure 21) has an insertion loss as low as 2.4 dB.

## 4 Conclusions

LioniX' TriPleX technology is a versatile photonics platform suited for applications over a wide wavelength range covering the transparency window from 0.4 to 2.35  $\mu\text{m}$ . Ultralow-loss channel waveguides with propagation losses down to 0.0005 dB/cm have been demonstrated. The monolithic integration of low- and high-contrast waveguides on the same chip enables the realization of low-loss spot-size converters. Therefore, TriPleX chips are suitable joints between different high-index platforms such as III-V or SOI and standard optical fibers giving access to the 'outside world'. Currently, substantial effort is put into the development of low-cost integration and assembly techniques for adding complementary functionalities of the different photonic platforms into a single package.

In this paper, we have reviewed a wide range of application examples that have been realized in or enabled by TriPleX technology. In the area of communications, components for telecommunication networks and microwave photonics operating in the 1.3- and 1.5- $\mu\text{m}$  wavelength window are discussed. High-performance filtering and true time delay concepts are surveyed, and components with high functional complexity for optical beam-forming networks are introduced. Milestones in the development of miniaturized biomedical devices can be mainly found in the field of optical coherence tomography and integrated Raman spectroscopy. The results addressed in this paper cover functional devices operating over a broad spectral range, from VIS to 1.3  $\mu\text{m}$ . Although results in this field are still preliminary, the potential of integrated optics solutions becomes clear. Finally, sensor devices and subsystems are addressed. Main application fields are environmental control, food/water safety, and security. The spectral range of interest is at a visible wavelength and at 850 nm due to access to low-cost VCSEL light sources. State-of-the-art sensing concepts developed on the TriPleX platform allow for detection limits around  $10^7$  RIU.

The functionality of the TriPleX platform is captured by verified basic building blocks and incorporated in the library of a design kit developed by LioniX and Phoenix Software. The availability of this library in combination with affordable manufacturing through MPW shuttle runs lowers the threshold for researchers and entrepreneurs to enter and exploit photonics technology.

**Acknowledgments:** The authors would like to thank R. Duer (iNDX Lifecare Inc.), C. Roeloffzen (SatraX BV), and J. van Kerkhof (XiO Photonics BV) for providing photographs of their commercial products based on TriPleX chip technology. Co-workers of the following research

groups and companies are acknowledged for the fruitful discussions and collaborations: Department of Electrical and Computer Engineering at the University of California Santa Barbara, Politecnico di Milano, SatraX BV, Telecommunication Engineering Group at the University of Twente, Morton Photonics Inc., Photonics Research Group at Ghent University, Biomedical Engineering and Physics Group at Amsterdam Medical Center, Department of Imaging Physics at Delft University of Technology, TNO, iNDX Lifecare Inc., Division of Information Transmission Systems and Material Technology at National Technical University of Athens, XiO Photonics BV, Laser Physics and Nonlinear Optics Group at the University of Twente, Phoenix BV.

## References

- [1] W. Sohler and R. De La Rue, Eds., *Laser Photonics Rev.* 6, Special Issue on Integrated Optics: From Single Photon Sources to Complex Photonic Circuits, (2012) pp. 1–143. <http://onlinelibrary.wiley.com/doi/10.1002/lpor.v6.1/issuetoc>.
- [2] W. Fritzsche and J. Popp, Eds., ‘Optical Nano- and Microsystems for Bioanalytics’, (Springer, Heidelberg, 2012) pp. 103–324.
- [3] <http://www.photonics21.org/AboutPhotonics21/workgroups.php>.
- [4] B. E. Little, S. T. Chu, W. Pan and Y. Kokubun, *IEEE Photonic Tech. L.* 12, 323 (2000).
- [5] C. K. Madsen, *J. Lightwave Technol.* 21, 2412 (2003).
- [6] [http://www.infinera.com/pdfs/whitepapers/Photonic\\_Integrated\\_Circuits.pdf](http://www.infinera.com/pdfs/whitepapers/Photonic_Integrated_Circuits.pdf).
- [7] J. Capmany and D. Novak, *Nat. Photonics* 1, 319 (2007).
- [8] D. Marpaung, C. Roeloffzen, R. Heideman, A. Leinse, S. Sales, et al., *Laser Photonics Rev.* 7, 506 (2013).
- [9] K. Okamoto, in ‘Proc. Asia Optical Fiber Communication Conf.’, (IEEE, Shanghai, October 17–19, 2007) pp. 307–309.
- [10] K. Wada, S. Park and Y. Ishikawa, *Proc. IEEE* 97, 1329 (2009).
- [11] M. Asghari, in ‘Proc. National Fiber Optic Engineers Conf.’, (IEEE, San Diego, February 24–28, 2008), paper NThA4.
- [12] L. Chen, K. Preston, S. Manipatruni and M. Lipson, *Opt. Express* 17, 15248 (2009).
- [13] J. Klamkin, F. Gambini, S. Faralli, A. Malacarne, G. Meloni, et al., *Opt. Express* 22, 2150 (2014).
- [14] V. M. N. Passaro, C. de Tullio, B. Troia, M. La Notte, G. Giannoccaro, et al., *Sensors* 12, 15558 (2012).
- [15] P. Kozma, F. Kehl, E. Ehrentreich-Förster, Ch. Stamm and F. F. Bier, *Biosens. Bioelectron.* 58, 287 (2014).
- [16] S. Janz, D. X. Xu, M. Vachon, N. Sabourin, P. Cheben, et al., *Opt. Express* 21, 4623 (2013).
- [17] N. Ismail, L.-P. Choo-Smith, K. Wörhoff, A. Driessen, A. C. Baclig, et al., *Opt. Lett.* 36, 4629 (2011).
- [18] V. D. Nguyen, B. I. Akka, K. Wörhoff, R. M. de Ridder, M. Pollnau, et al., *Opt. Lett.* 36, 1293 (2011).
- [19] G. Yurtsever, N. Weiss, J. Kalkman, T. G. van Leeuwen and R. Baets, *Opt. Lett.* 39, 5228 (2014).
- [20] <http://en.wikipedia.org/wiki/Infrared>.
- [21] M. Hoekman, J. Dingjan, P. J. Harmsma, R. P. Ebeling, D. M. R. Lo Cascio, et al., Poster in ‘ESA Round Table on Micro and Nano Technologies’ (2014).
- [22] <http://www.phoenixbv.com/index.php>.
- [23] <http://www.vlcp Photonics.com/mpw/>.
- [24] <http://www.oclaro.com/technology/photonic-integration/>.
- [25] [www.jeppix.eu](http://www.jeppix.eu), <http://paradigm.jeppix.eu/>.
- [26] <http://www.hhi.fraunhofer.de/fields-of-competence/photonic-components.html>.
- [27] <http://www.smartphotonics.nl/>.
- [28] <http://www.epixfab.eu/>, <http://www.europractice-ic.com/>.
- [29] <http://www.leti.cea.fr/en>.
- [30] <http://www.a-star.edu.sg/ime/>.
- [31] <http://www.lionixbv.nl/technology/technology-integrated-optics.html>.
- [32] R. G. Heideman, A. Leinse, W. Hoving, R. Dekker, D. H. Geuzebroek, et al., in ‘Proc. SPIE Vol. 7221’, (2009) pp. 72210R1.
- [33] C. G. H. Roeloffzen, L. Zhuang, C. Taddei, A. Leinse, R. G. Heideman, et al., *Opt. Express* 21, 22937 (2013).
- [34] L. Augustin, M. Smit, N. Grote, M. Wale and R. Visser, *Euro Photonics* article ID 54836 (2013), <http://www.photonics.com/Article.aspx?AID=54836>.
- [35] [http://www.mellanox.com/page/white\\_papers\\_silicon\\_photonics](http://www.mellanox.com/page/white_papers_silicon_photonics).
- [36] A. Leinse, R. G. Heideman, M. Hoekman, F. Schreuder, F. Falke, et al., in ‘Proc. SPIE Vol. 8767’, (SPIE, May 22, 2013) pp. 87670E-1.
- [37] R. Dekker, E. J. Klein and D. H. Geuzebroek, in ‘Proc. IEEE Photonics Conf.’, (IEEE, Burlingame, CA, 23–27 Sept. 2012) pp. 286–287.
- [38] R. G. Heideman and J. A. Walker, in ‘Proc. SPIE Vol. 6125’, (SPIE, Photonics West, San Jose, 2006) paper 021.
- [39] F. Morichetti, A. Melloni, M. Martinelli, R. G. Heideman, A. Leinse, et al., *J. Lightwave Technol.* 25, 2579 (2007).
- [40] R. G. Heideman, D. Geuzebroek, A. Leinse, A. Melloni, F. Morichetti, et al., in ‘Proc. ECIO’, (Copenhagen, April 25–27, 2007) invited paper WB0.
- [41] W. Hoving, D. Geuzebroek and R. Heideman, *SPIE Newsroom* 2008. <http://www.spie.org/x25303.xml?pf=true&highlight=x2414>.
- [42] R. G. Heideman, M. Hoekman and E. Schreuder, *IEEE J. Sel. Top. Quant.* 18, 1583 (2012).
- [43] R. G. Heideman, A. Melloni, M. Hoekman, A. Borreman, A. Leinse, et al., in ‘Proc. IEEE/LEOS Benelux Ann. Symp.’, (IEEE, Mons, December 1–2, 2005), pp. 71–74.
- [44] D. A. I. Marpaung, C. G. H. Roeloffzen, A. Leinse and M. Hoekman, *Opt. Express* 18, 27359 (2010).
- [45] G. Yurtsever, B. Považay, A. Alex, B. Zabihian, W. Drexler, et al., *Biomedical Opt. Express* 5, 1050 (2014).
- [46] L. Zhuang, D. Marpaung, M. Burla, W. Beeker, A. Leinse, et al., *Opt. Express* 19, 23162 (2011).
- [47] D. T. Spencer, M. J. R. Heck, R. Moreira, J. Bovington, J. E. Bowers, et al., in ‘Proc. OFC’, (OSA, San Francisco, March 9–14, 2014) paper Th1A.
- [48] J. F. Bauters, M. J. R. Heck, D. John, D. Dai, M. C. Tien, et al., *Opt. Express* 19, 3163 (2011).
- [49] D. Dai, Z. Wang, J. F. Bauters, M. C. Tien, M. Heck, et al. Bowers, in ‘Proc. GFP’, (IEEE, Beijing, September 1–3, 2010), P2.13.
- [50] J. F. Bauters, M. J. R. Heck, D. Dai, J. S. Barton, D. J. Blumenthal, et al., *IEEE Photonics J.* 5, 6600207 (2013).

- [51] J. F. Bauters, M. J. R. Heck, D. D. John, J. S. Barton, C. M. Bruinink, et al., *Opt. Express* 19, 24090 (2011).
- [52] J. F. Bauters, M. J. R. Heck, D. D. John, M.-C. Tien, W. Li, et al., in 'Proc. ECOC', (OSA, Geneva, September 18–22, 2011) paper Th12.3.
- [53] J. P. Epping, M. Hoekman, R. Mateman, A. Leinse, R. G. Heideman, et al., *Opt. Express* 23, 643 (2015).
- [54] M. J. Wale, Roadmap for InP and TriPleX-based Photonic Integration, presented at 5th European Photonic Integration Forum, ECOC Workshop: Low-Cost Access to Photonic ICs (London, 22nd September 2013).
- [55] M. J. R. Heck, J. F. Bauters, M. L. Davenport, D. T. Spencer and J. E. Bowers, *Laser Photonics Rev.* 8, 667 (2014).
- [56] D. Dai, J. Bauters and J. E. Bowers, *Light Sci. Appl.* 1, 1 (2012).
- [57] M. Piels, J. F. Bauters, M. L. Davenport, M. J. R. Heck and J. E. Bowers, *J. Lightwave Technol.* 32, 817 (2014).
- [58] M. Davenport, J. Bauters, M. Piels, A. Chen, A. Fang, et al., in 'Proc. NFOEC', (OSA, Anaheim, March 17–21, 2013) paper PDP2C.5.
- [59] EU FP7 project PHASTFlex (<http://www.phastflex.eu/>).
- [60] R. G. Heideman and M. Hoekman, Two-dimensional tapered coupler (nonlinear taper), U.S. Patent Application No.: 14/270,014.
- [61] J. Yue, F. H. Falke, J. C. Schouten and T. A. Nijhuis, *Lab Chip* 13, 4855 (2013).
- [62] <http://www.lionixbv.nl/triplexmpw.html>.
- [63] <http://www.actphast.eu/>.
- [64] T. J. Kippenberg, S. M. Spillane and K. J. Vahala, *Appl. Phys. Lett.* 85, 6113 (2004).
- [65] D. T. Spencer, Y. Tang, J. F. Bauters, M. J. R. Heck and J. E. Bowers, in 'Proc. IEEE Photonics Conf.', (IEEE, Burlingame, 2012) pp. 141–142.
- [66] D. T. Spencer, J. F. Bauters, M. J. R. Heck and J. E. Bowers, *Optica* 1, 153 (2014).
- [67] M. C. Tien, J. F. Bauters, M. J. R. Heck, D. T. Spencer, D. J. Blumenthal, et al., *Opt. Express* 19, 13551 (2011).
- [68] D. Dai, Z. Wang, J. F. Bauters, M. C. Tien, M. J. R. Heck, et al., *Opt. Express* 19, 14130 (2011).
- [69] L. Zhuang, W. P. Beeker, A. Leinse, R. G. Heideman and C. G. H. Roeloffzen, *Opt. Express* 21, 3114 (2013).
- [70] L. Zhuang, M. R. Khan, W. P. Beeker, A. Leinse, R. G. Heideman, et al., *Opt. Express* 20, 26499 (2012).
- [71] M. Burla, D. A. I. Marpaung, L. Zhuang, C. G. H. Roeloffzen, M. R. Khan, et al., *Opt. Express* 19, 21476 (2011).
- [72] D. A. I. Marpaung, L. Chevalier, M. Burla and C. G. H. Roeloffzen, *Opt. Express* 19, 24839 (2011).
- [73] D. Marpaung, B. Morrison, R. Pant, C. Roeloffzen, A. Leinse, et al., *Opt. Express* 21, 23286 (2013).
- [74] C. G. H. Roeloffzen, R. M. Oldenbeuving, R. B. Timens, P. W. L. van Dijk, C. Taddei, et al., in 'Proc. Optical Fiber Communication Conf.', (OSA, Los Angeles, March 22–26, 2015), invited paper Tu3F.4.
- [75] M. Burla, D. Marpaung, L. Zhuang, M. Khan, A. Leinse, et al., *J. Lightwave Technol.* 32, 3509 (2014).
- [76] L. Zhuang, C. G. H. Roeloffzen, A. Meijerink, M. Burla, D. A. I. Marpaung, et al., *J. Lightwave Technol.* 28, 19 (2010).
- [77] P. A. Morton, J. B. Khurgin, Z. Mizrahi and S. J. Morton, in 'Proc. CLEO', (OSA, San Jose, June 8–13, 2014) paper AW3P.6.
- [78] P. A. Morton, J. B. Khurgin, Z. Mizrahi and S. J. Morton, in 'Proc. Avionics, Fiber-Optics and Photonics Technology Conf.', (IEEE, Atlanta, GA, USA, 2014), pp. 27–28.
- [79] R. L. Moreira, J. Garcia, W. Li, J. Bauters, J. S. Barton, et al., *IEEE Phot. Tech. L.* 25, 1165 (2013).
- [80] L. Zhuang, M. Hoekman, C. Taddei, A. Leinse, R. G. Heideman, et al., *Opt. Express* 22, 17079 (2014).
- [81] C. Taddei, L. Zhuang, M. Hoekman, C. Roeloffzen, R. Oldenbeuving, et al., in 'Proc. International Topical meeting on Microwave Photonics/The 9th Asia-Pacific Microwave Photonics Conf.', (IEEE, Sapporo, Japan, 20–23 October 2014) paper TuC-4.
- [82] V. D. Nguyen, N. Weiss, W. Beeker, M. Hoekman, A. Leinse, et al., *Opt. Lett.* 37, 4820 (2012).
- [83] M. Boerkamp, T. van Leest, J. Heldens, A. Leinse, M. Hoekman, et al., *Opt. Express* 22, 30528 (2014).
- [84] <http://www.xiophotonics.com/index.php/hyperion-integrated-multi-color-laser-source>.
- [85] P. V. Lambeck, *Meas. Sci. Technol.* 17, R93 (2006).
- [86] E. Verdult, *NanoNextNL magazine* 1, 16 (2013), <http://www.nanonextnl.nl/>.
- [87] R. G. Heideman, R. P. H. Kooyman and J. Greve, *Sensor Actuat B-Chem* 10, 209 (1993).
- [88] A. Brandenburg, R. Edelhäuser and F. Hutter, *Sensor Actuat B-Chem* 11, 361 (1993).
- [89] K. De Vos, I. Bartolozzi, E. Schacht, P. Bienstman and R. Baets, *Opt. Express* 15, 7610 (2007).
- [90] D. X. Xu, A. Densmore, A. Delâge, P. Waldron, R. McKinnon, et al., *Opt. Express* 16, 15137 (2008).
- [91] K. Misiakos, I. Raptis, A. Salapatras, E. Makarona, A. Botsialas, et al., *Opt. Express* 22, 8856 (2014).
- [92] B. J. Luff, J. S. Wilkinson, J. Pihler, U. Hollenbach, J. Ingenhoff et al., *J. Lightwave Technol.* 16, 583 (1998).
- [93] A. Densmore, D. X. Xu, P. Waldron, S. Janz, P. Cheben, et al., *IEEE Phot. Tech. L.* 18, 2520 (2006).
- [94] L. Gounaridis, P. Groumas, E. Schreuder, R. Heideman, V. Katopodis, et al., *Sensor Actuat. B-Chem.*, 209, 1057 (2015).
- [95] iNDx lifecare (<http://indxlifecare.com/>).
- [96] R. Duer, R. Lund, R. Tanaka, D. A. Christensen and J. N. Herron, *Anal. Chem.* 82, 8856 (2010).
- [97] A. Prak, H. Leeuwis, R. G. Heideman, A. Leinse and G. Borst, in 'Proc. SPIE Vol. 7928', (SPIE, San Francisco, January 22, 2011) paper L-1.
- [98] M. Belt, J. Bovington, R. Moreira, J. F. Bauters, M. J. R. Heck, et al., *Opt. Express* 21, 1181 (2013).
- [99] M. Belt and D. J. Blumenthal, *Opt. Express* 22, 10655 (2014).
- [100] R. M. Oldenbeuving, E. J. Klein, H. L. Offerhaus, C. J. Lee, H. Song, et al., *Phys. Lett.* 10, 015804 (2013).
- [101] J. P. Epping, T. Hellwig, R. Mateman, A. van Rees, M. Hoekman, et al., in 'Proc. Of 6th EPS-QEOD Europhoton Conf.', (OSA, Neuchâtel, Switzerland, August 24–29, 2014).
- [102] J. P. Epping, M. Kues, P. J. M. van der Slot, C. J. Lee, C. Fallnich, et al., *Opt. Express* 21, 32123 (2013).
- [103] R. P. Ebeling, P. J. Harmsma, D. M. R. Lo Cascio, M. Hoekman, W. P. Beeker, et al., in 'Proc. IEEE/LEOS Benelux Ann. Symp.', (IEEE, Mons, November 29–30, 2012) pp. 109–112.



**Kerstin Wörhoff**  
LioniX BV, Enschede, P.O. Box 456, 7500 AL,  
The Netherlands,  
k.worhoff@lionixbv.nl

Kerstin Wörhoff received a MSc degree in Electrical Engineering and a PhD degree in Applied Physics in 1991 and 1996, respectively. Between 1996 and 2000 she worked as a Postdoctoral researcher at the Lightwave Devices group of the University of Twente with research focus on photonics technology development for telecom applications. In 2000 she obtained an assistant professor position in Integrated Optics at the University of Twente and was involved in various European as well as national research projects. Her expertise includes development and optimization of photonics technologies for a wide range of active and passive integrated optical functionalities, optical waveguide design as well as project management and teaching in Materials Science and Technology. In 2013 she joined LioniX BV as a project manager and design engineer.



**René Heideman**  
LioniX BV, Enschede, P.O. Box 456, 7500 AL,  
The Netherlands

René Heideman received the MSc and PhD degrees in Applied Physics from the University of Twente (Enschede, The Netherlands) in August 1988 and January 1993, respectively. He is an expert in the field of MST, based on more than 25 years of experience. He has specialized in Integrated Optics (IO), covering both (bio-) chemical sensing and telecom applications. He is (co)author of more than 200 papers and holds more than 20 patents in the IO-field, on more than 10 different subjects. Since 2001, he is co-founder and CTO of LioniX BV. Since 2008, he is CTO of Panthera, a group of high-tech innovative companies focusing on creating new business based on micro/nano-technology. He is member of several Dutch steering committees, IEEE BioPhotonics and the board of stakeholders of Photonics21. He is also Board member of MinacNed (Dutch association for micro-systems and nanotechnology). Since 2012, René Heideman is a (visiting) professor Nanotechnology of Saxion University of Applied Sciences.



**Arne Leinse**  
LioniX BV, Enschede, P.O. Box 456, 7500 AL,  
The Netherlands

Arne Leinse (Project-/account manager & Vice President) received a MSc degree from the University of Twente in the Integrated Optical Microsystems group in 2001. In this same group he started his PhD work on the topic of active micro-ring resonators for various optical applications. His PhD work was carried out in the framework of a European project (IST 2000-28018 “Next generation Active Integrated optic Sub-systems”) and his thesis was titled: “Polymeric micro-ring resonator based electro-optic modulator”. In 2005 he joined LioniX BV where he is now as a project-/account manager involved in several integrated optical projects, member of the management team and involved in the strategic roadmap of the technology and LioniX.



**Marcel Hoekman**  
LioniX BV, Enschede, P.O. Box 456, 7500 AL,  
The Netherlands

Marcel Hoekman was born in Zutphen, The Netherlands, in 1974. He received the MSc degree in Applied Physics and the MTD degree in Integrated Optics from the University of Twente, Enschede, The Netherlands, in 1998 and 2001, respectively. From 1998 to 2001 he worked on his post graduate design program in the Integrated Optical MicroSystems Group at the University of Twente. He worked on the design of an integrated optical/electro-optical modulator based on PZT containing multi-layer stacks. In this project he collaborated with the group Experimental Solid State Physics III of Radboud University Nijmegen. From 2004 until 2009 he has been a part-time PhD student at the Integrated Optical MicroSystems Group of the University of Twente, in the framework of the STW project “Multi-Sensing Arrays of Separately Accessible Optics Sensors”. In 2001 he joined Lion Photonix Technologies B.V., Enschede, The Netherlands - which has continued as LioniX B.V. since 2002 - as a design engineer. Besides simulation and mask design he has experience in several cleanroom manufacturing processes and characterization methods, and he has worked as internal project leader on several national and European projects.